Journal of MATERIALS RESEARCH

Invited Paper
DOI:10.1557/s43578-023-01226-z

Integration of galfenol into CoFeB magnetic tunnel junction electrodes

Suyogya Karki[1,2], Joe Davies[3], Matthew H. Kane[3], Supriyo Bandyopadhyay[4], Jean Anne C. Incorvia[1,2,a)]

[1] Department of Electrical and Computer Engineering, The University of Texas at Austin, 2501 Speedway, Austin, TX 78712, USA
[2] Microelectronics Research Center, The University of Texas at Austin, 10100 Burnet Rd, Austin, TX 78758, USA
[3] NVE Corporation, 11409 Valley View Rd, Eden Prairie, MN 55344, USA
[4] Department of Electrical and Computer Engineering, Virginia Commonwealth University, 601 W Main St, Richmond, VA 23284, USA
[a)] Address all correspondence to this author. e-mail: incorvia@austin.utexas.edu

Received: 3 August 2023; accepted: 7 November 2023

Mechanical strain provides a knob for controlling the magnetization of the magnetostrictive-free layer of magnetic tunnel junctions (MTJs), with many applications for energy-efficient memory and computing. This requires integrating materials with high magnetostriction coefficient into MTJs, while still preserving the CoFeB-MgO tunnel barrier for high tunnel magnetoresistance (TMR). One way to accomplish this is to replace the CoFeB free layer of the MTJ with an exchange-coupled bilayer of CoFeB and a highly magnetostrictive ferromagnet like Galfenol (FeGa). Here, FeGa, a thermally stable magnetostrictive material, is integrated into CoFeB-based MTJs. We show that engineering a thin layer of CoFeB and FeGa provides a means of controlling the magnetic properties and switching field in FeGa-based MTJs, and that the exchange-coupled FeGa-CoFeB layer can be used as both a free layer and a fixed layer in the MTJ stack with TMR as high as 100%.

Introduction

Magnetoelectric multiferroics have gained interest due to the dynamic and controllable coupling between magnetization and charge degrees of freedom in these materials. Such magnetoelectric multiferroics can be engineered by interfacing magnetostrictive thin films with piezoelectrics, and would enable ultrafast, voltage-induced switching of magnetization [1–3]. Controlling magnetism with electric fields allows for novel device architectures for several applications such as sensors [4], energy harvesters [5], and memory [6]. One such use for engineered magnetoelectric heterostructures is to integrate them into magnetic tunnel junctions (MTJs). MTJs are thin-film stacks consisting of a thin-insulating layer sandwiched between two ferromagnetic layers that are a cornerstone of spintronics, with use in memory [7], logic [8], neuromorphic computing [9–11], and probabilistic computing [12, 13]. The magnetization of the lower coercivity-free layer(s) ferromagnetic electrode relative to the higher-coercivity fixed layer(s) ferromagnetic electrode encodes a nonvolatile higher (bit 1) or lower (bit 0) resistance state. The MTJ is characterized by the tunnel magnetoresistance $TMR = \frac{R_{AP}-R_P}{R_P} \times 100\%$ and the resistance-area product $RA = R_P \times A$, where A is the cross-sectional area of the junction. MgO tunnel barriers [14, 15] with CoFeB ferromagnetic electrodes are state of the art for high-performance MTJs. Magnetic field, spin-transfer torque, and spin–orbit torque are mechanisms used to switch the free layer in MTJs [16]. However, if the free layer of the MTJ structure is integrated as a magnetostrictive layer interfaced with a piezoelectric layer and switched via strain induced from electric field, it leads to 1000 times lower energy switching compared to standard spin-transfer torque switching in MTJs [17] and at least 10 times lower switching energy compared to voltage-controlled switching of MTJs [18]. Strain can also be used in conjunction with other switching methods to increase the tunability of the MTJ resistance states, for example for use in probabilistic computing [19].

When strain is applied to a material, magnetic anisotropy is induced in the material which results in a change in the direction of magnetization. This behavior is known as inverse magnetostriction or Villari effect. The energy required to switch a ferromagnetic layer completely via strain is given by $E_b = \frac{3}{2}\lambda_s \sigma_{min} \Omega$, where λ_s is the magnetostriction coefficient, σ_{min} is the minimum strain required, and Ω is the volume of the

free layer. Therefore, for enhancing the strain-based switching of the ferromagnetic layer, one approach is to study materials with larger λ_s leading to smaller σ_{min} requirement, and thus, requiring smaller voltages. This motivates us to explore and study the properties of ferromagnetic materials with high λ_s and their compatibility with MTJs.

Transition metal ferromagnets like Co, Fe, and their alloys, like CoFeB, are commonly used as the ferromagnetic electrode in state-of-art MTJs due to their high spin polarization, low damping, and lattice match with the MgO tunnel barrier resulting in high TMR [14, 15]. However, these alloys exhibit relatively modest bulk magnetostriction coefficients of the order 10–60 ppm [20], while still showing some possibility for magnetoelectric switching when interfaced with a piezoelectric but demonstrates higher strain requirement [21–23]. There have been previous studies to explore properties of materials with high λ_s like FeGa [24] and Terfenol-D [25]. Terfernol-D has the highest magnetostriction coefficient of ~ 500 ppm, but it is a quaternary alloy with multiple phases, which presents challenges to depositing nanometer thin films. In contrast, the binary alloy $Fe_{0.81}Ga_{0.19}$ demonstrates magnetostriction coefficient ~ 300 ppm [26], over ten times higher than those of transition metal ferromagnets and has been successfully sputter deposited. Previous studies of the electronic properties of FeGa show that there is an increase in spin–orbit coupling interactions among local states in Fe with addition of Ga atoms, thereby enhancing the magnetostriction [26]. Recent experimental studies have also confirmed that $Fe_{0.81}Ga_{0.19}$ films exhibit exceptionally low gilbert damping ($\alpha = 0.012$) and a significant magneto-mechanical coupling [27]. The high magnetostriction coefficient and low damping exhibited by FeGa makes it an exciting material choice for electrodes in straintronic MTJs, as it would enable a stronger magnetoelectric (ME) coupling. FeGa also has an excellent thermal stability with a high Curie temperature of 675 °C [28]. While the inclusion of Gallium in Fe is responsible for the increased magnetostriction, it is important to note that the addition of Gallium presents challenges when used as an ultra-thin layer in an MTJ thin-film stack. One significant challenge is the low melting point of Gallium, which is approximately 29 °C [29]. This makes FeGa a challenging material to integrate into MTJ devices where post-ultra-high-vacuum (UHV) annealing is essential for achieving high *TMR* junctions. Therefore, while FeGa is promising for ferromagnetic electrodes for strain-based devices, no work has integrated FeGa into CoFeB MTJs while still preserving a robust *TMR*. Therefore, a detailed study of growth conditions, characterization, and optimization of thin layers of FeGa integrated into MTJs is needed.

In this work, we study low-energy-barrier, thermally stable magnetostrictive Galfenol ($Fe_{0.81}Ga_{0.19}$) and its integration with $Co_{20}Fe_{60}B_{20}$ ferromagnetic electrodes in MTJ thin-film stacks. We start with characterizing the growth conditions, crystal orientation, and magnetic properties of the FeGa films. Subsequently, an ultra-thin layer consisting of FeGa | CoFeB is engineered as a ferromagnetic electrode material. This layer is studied for performing as both the free and fixed layers of an MTJ, showing that FeGa can pin a ferromagnetic layer without use of a complex synthetic antiferromagnet (SAF) thin-film stack. This is a direct manifestation of exchange coupling between the FeGa layer and CoFeB layer [30]. The latter part of this work focuses on the characterization of different MTJ stacks under various UHV annealing conditions. Our results suggest that optimizing the thickness of CoFeB and FeGa provides a means of controlling the magnetic properties and switching field in FeGa-based MTJs via exchange coupling of the FeGa | CoFeB layer. In addition, the introduction of a thin Ru spacer layer between CoFeB and FeGa, along with optimization of post-UHV annealing conditions, effectively mitigates gallium diffusion and improves the *TMR* in the MTJs. Transmission electron microscopy (TEM) results show a well-defined interface between MgO and CoFeB, with polycrystalline FeGa. Therefore, this study provides a comprehensive analysis of the growth, properties, and performance of FeGa films, as well as the development and characterization of MTJ stacks incorporating both FeGa and CoFeB materials for application in straintronics.

Results and discussion

Galfenol films with thicknesses of 10 nm, 30 nm, and 80 nm were deposited via sputtering onto silicon (substrate)|100 nm SiO_2.The magnetic properties of the films are studied using a vibrating sample magnetometer (VSM). Figure 1(a) shows the in-plane hysteresis loop of the films. The volume saturation magnetization for 10 nm, 30 nm, and 80 nm films is 74 $\frac{kA}{m}$, 95 $\frac{kA}{m}$, and 94 $\frac{kA}{m}$, respectively. The coercivity of the films ranges from 4.1 mT to 5.5 mT as shown in Fig. 1(b), ultimately showing that the coercivity is approximately constant with respect to thickness. This suggests that the growth conditions are optimum, and that the intrinsic magnetic properties of the films are relatively stable [27]. To further understand the properties of sputtered films, X-ray diffraction (XRD) is used to study the crystal orientation of the 30 nm film. Figure 1(c) shows the out-of-plane XRD diffraction pattern, which shows that the preferred crystal orientations are in the (110) directions for high magnetostriction of FeGa alloy. The interplanar distance is calculated to be 2.05 Å, with $2\theta = 44.5°$.

FeGa by itself might not be a sufficient electrode material for high on/off ratio in MTJs, since well-defined Δ_1-symmetry states near the Fermi energy are not studied in detail and polycrystalline grain boundaries reduce *TMR*[31]. Therefore, engineering a coupled FeGa | CoFeB magnetic layer is essential to achieve junctions with high magnetostriction and an acceptable *TMR*.

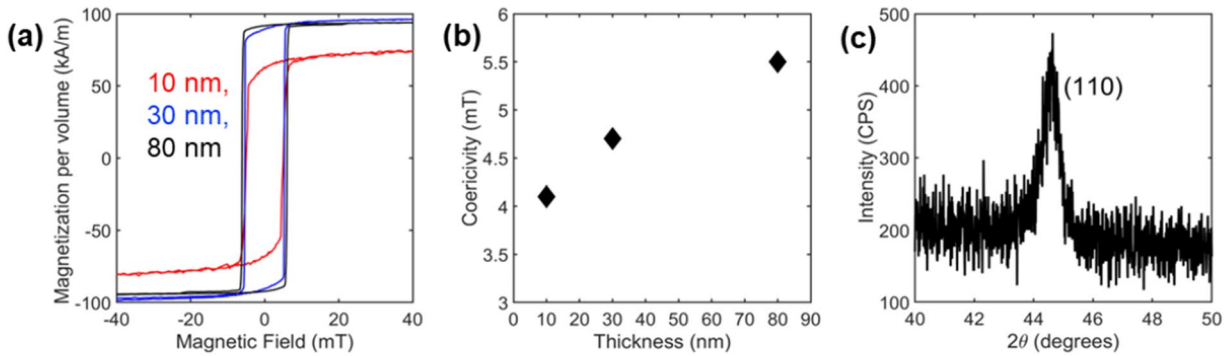

Figure 1: Characterization of FeGa thin films. (a) In-plane magnetic hysteresis loop of FeGa films for 10 nm, 30 nm, and 80 nm thickness. (b) Coercivity vs thickness of FeGa films. (c) XRD data for the 30 nm FeGa film.

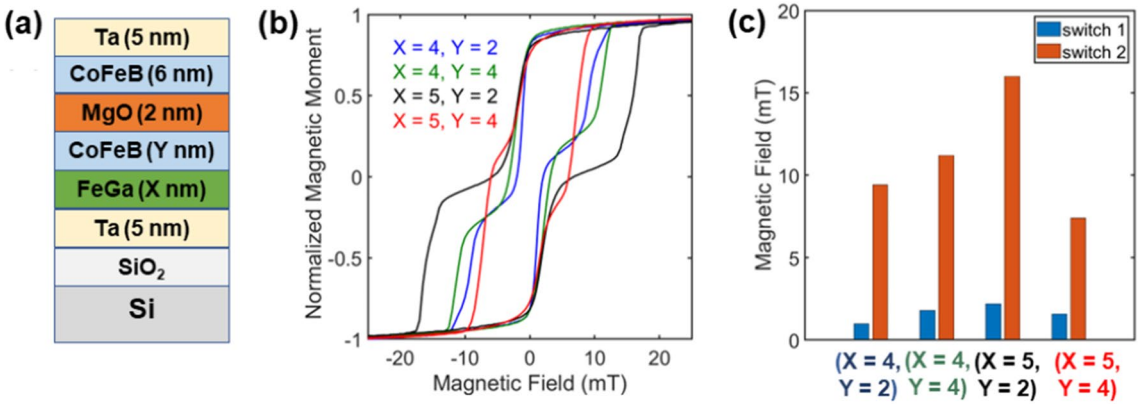

Figure 2: (a) MTJ stack; X and Y represent thickness of FeGa and CoFeB, respectively, in nm. (b) In-plane magnetic hysteresis loops of the FeGa MTJ stacks with varied X and Y. (c) Switching fields for the MTJ stacks.

Figure 2 shows our results integrating the FeGa into the CoFeB ferromagnetic layer of MTJs. Figure 2(a) depicts the grown MTJ stacks, where X and Y represent various thicknesses of FeGa and CoFeB, respectively. Several samples of FeGa|CoFeB are sputtered, but here, we study and discuss magnetic properties for four exemplar MTJ stacks. In these MTJ stacks, the 5 nm bottom Ta layer is used as an adhesion layer; the top 5 nm Ta as a protective capping layer to prevent degradation of the top 6 nm CoFeB layer on top of the 2 nm MgO tunnel barrier. Four different combinations of bottom CoFeB and FeGa thicknesses are studied: 4 nm FeGa with 2 nm CoFeB, 4 nm FeGa with 4 nm CoFeB, 5 nm FeGa with 2 nm CoFeB, and 5 nm FeGa with 4 nm CoFeB. In-plane magnetic hysteresis for the various stacks is shown in Fig. 2(b). The blue and green hysteresis loop for $X = 4$, $Y = 2$ and $X = 4$, $Y = 4$ shows similar switching fields of the ferromagnetic layers. The red hysteresis curve shows that for $X = 5$ and $Y = 4$, the two switches are slightly distinguishable, but the field range between switches is smaller compared to the previous two stacks. For the stack with FeGa $X = 5$ and CoFeB $Y = 2$, the magnetic hysteresis shows a distinct switching mechanism as shown in the black hysteresis loop. Figure 2(c) shows the switching field values for the top CoFeB layer labeled as switch 1, along with the coupled FeGa|CoFeB layer labeled as switch 2. For all the samples, the top CoFeB layer switches within a range of 1 mT to 2.2 mT, showing that the free layer switching is independent of the bottom FeGa|CoFeB layer switching. For the stacks $X = 4$, $Y = 2$, and $X = 4$, $Y = 4$, the switching field is measured to be 9.4 mT and 9.8 mT, respectively. These results show that 4 nm FeGa exhibits dominant coercivity and effectively couples with both 2 nm and 4 nm CoFeB layers. For the sample with $X = 5$ and $Y = 2$, the two switches are 2.2 mT and 16 mT. These values suggest that the FeGa|CoFeB is well coupled and switches at a larger field compared to the free layer inner switch. The top CoFeB in all of the MTJ stacks is soft and switches at low field shown by the inner switch. Here, a thicker FeGa layer with higher coercivity influences the switching behavior of the bottom CoFeB layer, causing it to switch at a larger field along with the FeGa layer. In the stack with $X = 5$ and $Y = 4$, the values of switch 1 and switch 2 are 1.6 mT and 7.4 mT. Here, we notice that the FeGa|CoFeB switch has come in a lot towards the free layer switch as shown in red curve in Fig. 2(b). This could be due to more diffusion or intermixing resulting from thicker FeGa

and CoFeB layers, as well as from loss of Boron during the intermixing. These results suggest that optimizing the thickness of CoFeB and FeGa provides a means of controlling the magnetic properties and switching field in FeGa-based MTJs via exchange coupling of the FeGa|CoFeB layer.

UHV annealing of MTJs post-deposition is essential to achieve high *TMR*, as the MgO | CoFeB interface is amorphous and becomes polycrystalline or crystalline, allowing desirable electronic properties, after annealing [32]. In this study, we conduct UHV annealing on the MTJ stacks under various temperatures. Figure 3(a) presents the in-plane hysteresis loop of the Substrate|Ta (5)|FeGa (5)|CoFeB (2)|MgO (2)|CoFeB (6)|Ta (5) stack, with the numbers indicating layer thicknesses in nm, at several annealing temperatures. All anneals are done for 1 h at a pressure of 10^{-8} *Torr*. The black hysteresis loop is the easy axis measurement of the sample as grown. The blue and green hysteresis loops show the magnetic properties of the films annealed at 225 °C and 250 °C, respectively. The FeGa|CoFeB coercivity has reduced, but the two switches are still distinguishable. When annealed at 270 °C (red curve), the two switches are almost indistinguishable. This suggests intermixing of the electrode layers during annealing, which would be undesirable for the symmetry-filtering properties of the MgO|CoFeB which permit large *TMR*.

To investigate the degradation of the two switches in the annealed samples, we performed ion milling on the 270 °C annealed MTJ stack. Figure 3(b) shows the endpoint detector data during etching, with the x-axis representing the etching time and the y-axis indicating the count of each element detected. During the etching, boron was detected at around 8 min, followed by Fe at approximately 10 min. A sharp peak of Mg appeared at around 11 min, accompanied by a shoulder peak from Gallium. This suggests that Gallium diffuses into the MgO layer during post-annealing of the sample, leading to intermixing of the layers, thus, potentially degrading *TMR* and reducing the magnetostriction coefficient from displaced Ga in the FeGa layer. Therefore, careful selection of annealing temperature and duration is crucial to preserve the desirable properties of the MTJs and prevent the unwanted diffusion and intermixing of layers.

To reduce gallium diffusion into the MgO layer and optimize the exchange coupling within the electrode, we insert a thin Ru spacer layer of thickness 0.8 nm at the bottom CoFeB and FeGa interface. The MTJ stack is sputtered with the following layers: Substrate|Ta (5)|FeGa (5)|Ru (0.8)|CoFeB (2)|MgO (~ 2)|CoFeB (6)|Ta (5). The stack is UHV annealed at 270 °C for 1 h. Figure 4(a) shows the in-plane hysteresis of the stacks without (blue) and with (red) the Ru spacer. The Ru spacer restores two distinct switches at 1.5 mT and 8 mT, indicating reduced intermixing of the ferromagnetic layers. This is corroborated by etching through the stack, Fig. 4(b). The top Ta layer was first etched through and detected at around 19 min, followed by Fe and Co at approximately 23 min. We observe a sharp peak of Mg at around 26 min of etched time with no shoulder peak of Gallium. This confirms that there is no diffusion of Ga at the MgO and ferromagnetic layer interface. A sharp Ga peak was observed at around 28 min after the second peak of Co and Fe, suggesting that insertion of a thin Ru layer helps prevent Ga diffusion. This shows that with Ru insertion, the FeGa-integrated MTJ can withstand higher annealing temperatures, necessary for increasing the *TMR*.

Structural analysis was performed to understand the microstructure and interface between layers in the MTJ structure. Figure 5(a) displays the TEM image of the annealed at 270 °C for 1-h MTJ stack with layers Substrate|Ta (5)|FeGa (5)|Ru (0.8)|CoFeB (2)|MgO (~ 2)|CoFeB (6)|Ta (5). In Fig. 5(a), we

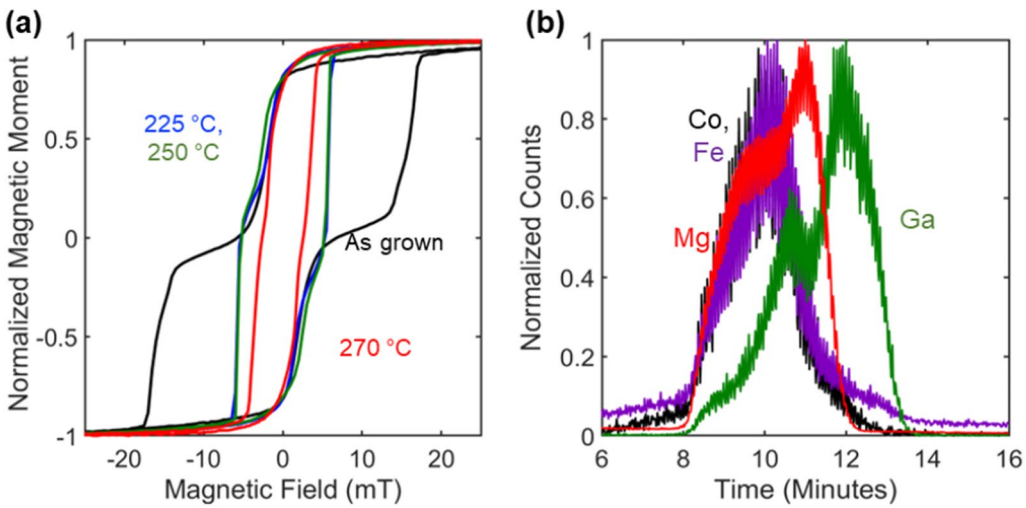

Figure 3: (a) In-plane magnetic hysteresis loops of the FeGa MTJ stacks, as grown and at different post-deposition UHV annealing temperatures. (b) Elemental analysis while etching through the layers in time, for the sample annealed at 270 °C.

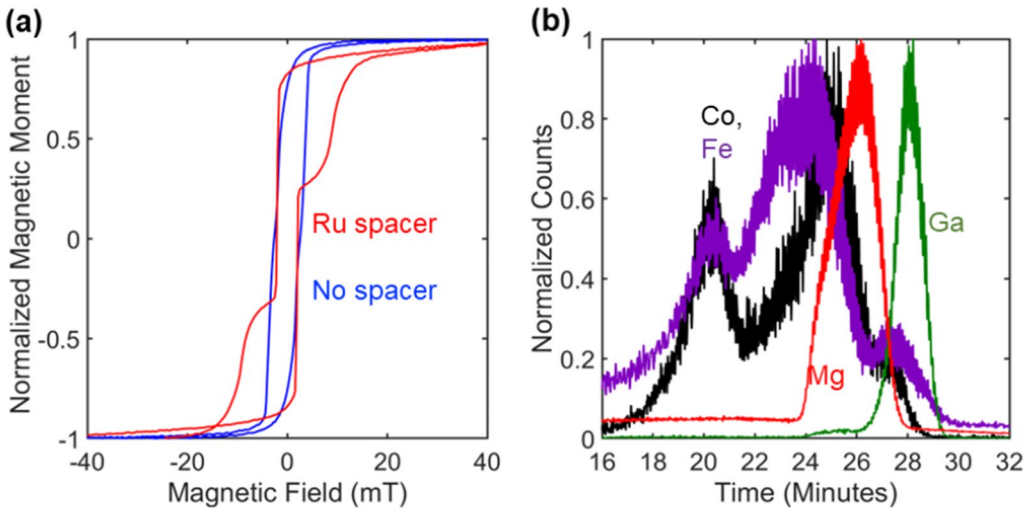

Figure 4: (a) In-plane magnetic hysteresis loops of the FeGa MTJ stacks, with and without Ru spacer at the FeGa/CoFeB interface. (b) Elemental analysis while etching through the layers in time, for the sample annealed at 270 °C with a Ru spacer.

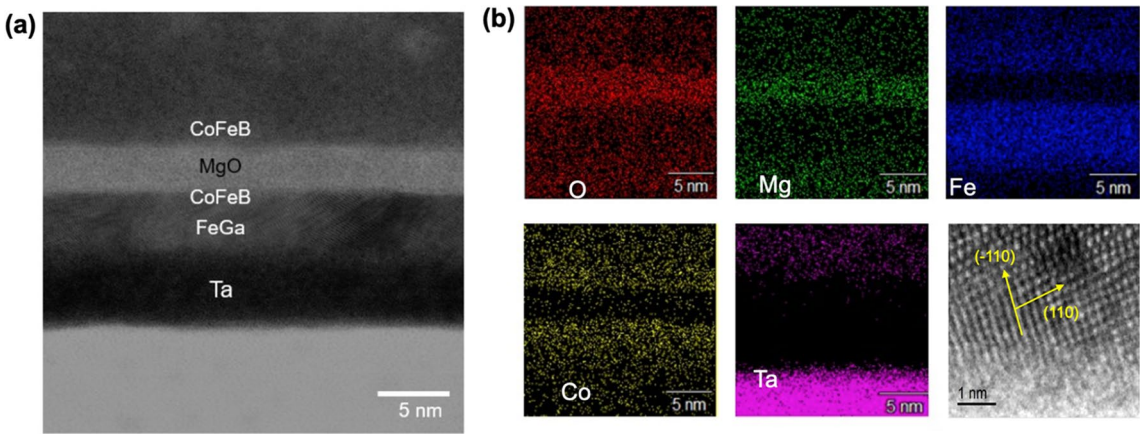

Figure 5: (a) Transmission electron microscopy image of the Ta (5)|FeGa (5)|Ru (0.8)|CoFeB (2)|MgO (2.5)|CoFeB (6)|Ta (5) MTJ stack; numbers in the bracket are in nm. (b) EDX elemental data analysis from the top to the bottom of the MTJ stack with a zoomed in TEM image of the FeGa layer.

observe that the MgO|CoFeB interface is sharp and that there is little diffusion of electrodes into the MgO layer, showing that with the Ru interlayer present, the FeGa is not creating grain boundaries or increasing roughness at the MgO interface. The MgO is observed to be amorphous, which could be due to the crystal structure of the FeGa-CoFeB bottom interface compared to a usual amorphous CoFeB bottom electrode [33]. The CoFeB layers are found to be partially polycrystalline. The 5 nm thin layer of FeGa is polycrystalline, as expected from our single-layer characterization of the films. Figure 5(b) shows the energy-dispersive X-ray (EDX) elemental mapping of O (red), Mg (green), Fe (blue), Co (yellow), and Ta (magenta) from top to the bottom of the MTJ structure. Due to Ga ions used to create the TEM lamella, Ga could not be directly observed. The Ru was too thin to be detected in EDX. It is evident that approximately 5 nm from the top, there is a distinct layer with higher concentrations of O (red) and Mg (green). At the interface of the Mg and O layer, we observe a thin layer with a higher concentration of Co which is evident in the yellow mapping, indicative that the CoFeB layer has adhered to the FeGa layer. In the elemental mapping of Fe, indicated by the blue color, there is high concentration of Fe for roughly ~ 7 nm below the MgO layer. This shows that Fe concentrations are both from the CoFeB and FeGa layers. The magenta color mapping represents the presence of the Ta below the FeGa layer.

Current in-plane tunneling (CIPT) [34] measurements were performed to measure the *TMR* for five different stacks, with results shown in Fig. 6(a). The *TMR* ranges from 11% to greater than 100%. Stacks 1, 3, and 4 correspond to the MTJ structure discussed in Fig. 4(a) without Ru spacer layer, and post-UHV annealed at 270 °C for 1 h, 300 °C for 1 h, and as grown, respectively. The *TMR* values of the three stacks are measured to be

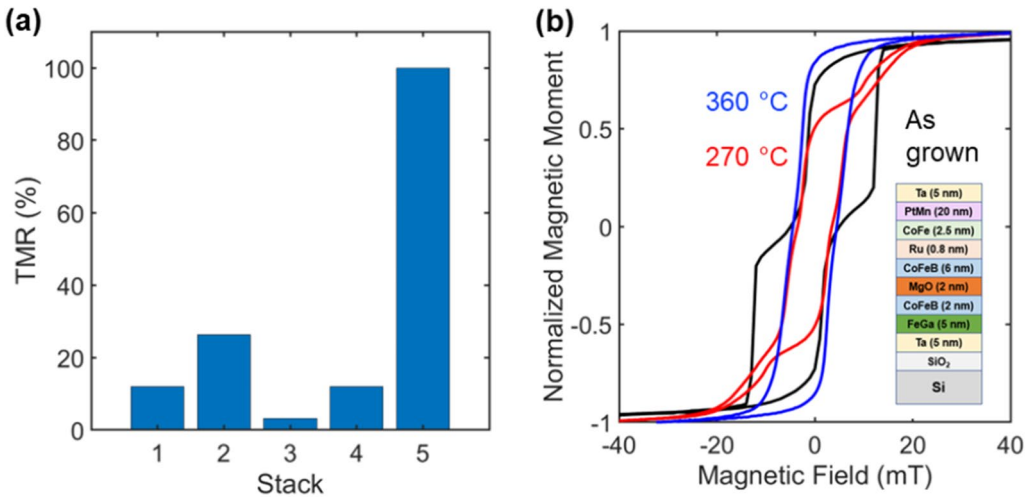

Figure 6: (a) *TMR* of the various FeGa MTJ stacks. (b) In-plane magnetic hysteresis loops for the SAF FeGa MTJs at various annealing temperatures. Inset depicts the stack.

11%, 3.2%, and 12%, respectively. These results further support the claim discussed earlier, which suggests that *TMR* deteriorates with increasing temperature due to higher diffusion of gallium at elevated temperatures. On the other hand, Stack 2 represents the MTJ structure discussed in Fig. 4(a), with the addition of a Ru spacer layer, post-UHV annealed at 270 °C for 1 h. This stack exhibits an enhancement of *TMR* to 26%. Our results indicate that the introduction of Ru between the CoFeB and FeGa interfaces enhances the *TMR* from 11% to 26% for samples post-UHV annealed at 270 °C for 1 h, showing reduction of Ga diffusion with a spacer layer. Therefore, a thin Ru spacer layer between FeGa|CoFeB is critical to withstand higher annealing temperatures and results in enhancement of *TMR*.

Stack 5 demonstrates *TMR* exceeding 100%. The structure of this stack is different than the ones discussed in the earlier sections. Stack 5 is a synthetic antiferromagnet (SAF) pinned FeGa MTJ stack, composed of Substrate|Ta (5)|FeGa (5)|CoFeB (2)|MgO (2)|CoFeB (6)|Ru (0.8)|CoFe (2.5)|PtMn (20)|Ta (5). The SAF structure consists of CoFeB (6)|Ru (0.8)|CoFe (2.5)|PtMn (20) as the top-fixed electrode layer, and FeGa|CoFeB as the bottom-free layer of the MTJ. Figure 6(b) shows the in-plane hysteresis loop of the stack at different post-annealing conditions, including as grown, 270 °C for 1 h, and 360 °C for 1 h, with an in-plane applied magnetic field of 250 mT during annealing. The hysteresis loop shows that the sample at 270 °C reveals the presence of two outer loops, a characteristic of the pinned SAF layer [35], which helps keep the switching of the two layers distinct, promoting higher TMR [36]. Therefore, including a SAF-pinned layer allows for the FeGa|CoFeB electrode to be the free layer in these junctions, while still having high *TMR*, for use in strain-controlled applications.

Conclusion

In this work, we show that by optimizing both FeGa and CoFeB, we can create a coupled FeGa|CoFeB electrode and control its switching field and coercivity in MTJ thin-film stacks. The FeGa|CoFeB is shown to operate as both the fixed and free layer of the MTJ, showing that FeGa can pin a ferromagnetic layer without use of a complex synthetic antiferromagnet (SAF) thin-film stack, or can be used with a SAF to then manipulate the FeGa-based free layer with strain, while not sacrificing *TMR*. Magnetoresistance measurements show *TMR* as high as 100% in these junctions. These results show that FeGa with CoFeB can be considered as a promising magnetic electrode for MTJ-based magnetic devices and paves the way for incorporating them onto piezoelectric substrates, where a challenge is potentially higher substrate roughness compared to silicon.

Methods

An AJA Orion sputter system with base pressure $1.0 \times 10^{-8} Torr$ is used for the thin-film growths. An argon flow rate of 33 standard cubic centimeters per minute (sccm) is used for all sputtering processes, with DC sputtering for the metals and RF for the insulator. The FeGa films are sputtered from a composite FeGa target using a power of 60 Watts at an Argon pressure of 3 *mTorr*. The surface roughness of the FeGa films was measured via atomic force microscopy to be less than 1 nm. The growth condition of MgO was optimized to obtain 001 crystal orientation (see Supplemenatry Information). The CoFeB was sputtered using a composite target of 20:60:20 (atomic %) and post-UHV annealed. UHV annealing is performed using the same tool at a base pressure of $1.0 \times 10^{-8} Torr$.

Hysteresis loops are measured using a Microsense-vibrating sample magnetometer (VSM). XRD is performed using a Rikagu Ultmia IV to determine the crystallinity of the films. In-plane and out-of-plane measurements are used to measure the 2θ and 2θ-ω angles of the sputtered film. TEM is performed using a JEOL NEOARM Low kV STEM Corrected tool to study the nanostructure of the MTJ films, with lamella prepared using a Scios 2HiVac focused ion beam tool. Elemental mapping using EDX is performed during the TEM analysis of the film. An AJA ion miller is used to etch the stack, and the inbuilt secondary ion mass spectroscopy is employed to analyze the counts of the etched ions. *TMR* of the sputtered films is measured using a Smartprober TT CIPT tool at NVE corporation.

Acknowledgments

The authors acknowledge funding support from the National Science Foundation Division of Computing and Communication Foundations (NSF CCF) under Grant Numbers 2006753 (S. K., J. A. I.) and 2006843 (S. B.). The authors acknowledge the use of shared research facilities supported in part by the Texas Materials Institute and the Texas Nanofabrication Facility supported by NSF Grant No. NNCI-1542159.

Author contributions

SK conducted the experiments and prepared the manuscript. JD and MK provided discussions and helped with characterization of thin films. SB provided ideas and discussions of importance to the work. JACI created, led, and supervised the work and manuscript.

Data availability

The datasets generated during and/or analyzed during the current study are available from the corresponding author on reasonable request.

Declarations

Conflict of interest On behalf of all authors, the corresponding author states that there is no conflict of interest.

Supplementary Information

The online version contains supplementary material available at https://doi.org/10.1557/s43578-023-01226-z.

References

1. S. Bandyopadhyay, *Magnetic straintronics: an energy-efficient hardware paradigm of digital and analog information processing. synthesis lectures on engineering, science and technology* (Springer Nature, Berlin, 2022)
2. H. Ahmad, J. Atulasimha, S. Bandyopadhyay, Reversible strain-induced magnetization switching in FeGa nanomagnets: Pathway to a rewritable, non-volatile, non-toggle, extremely low energy straintronic memory. Sci. Rep. **5**(November), 1 (2015)
3. N.A. Spaldin, R. Ramesh, Advances in magnetoelectric multiferroics. Nat. Mater. **18**(3), 203 (2019)
4. M. Li, C. Dong, H. Zhou, Z. Wang, X. Wang, X. Liang, Y. Lin, N.X. Sun, Highly sensitive DC magnetic field sensor based on nonlinear ME effect. IEEE Sensors Lett. **1**(6), 18 (2017)
5. S. Dong, J. Zhai, J.F. Li, D. Viehland, S. Priya, Multimodal system for harvesting magnetic and mechanical energy. Appl. Phys. Lett. (2008). https://doi.org/10.1063/1.2982099
6. T. Kosub, M. Kopte, R. Hühne, P. Appel, B. Shields, P. Maletinsky, R. Hübner, M.O. Liedke, J. Fassbender, O.G. Schmidt, D. Makarov, Purely antiferromagnetic magnetoelectric random access memory. Nat. Commun. **8**, 1 (2017)
7. S. Chung, K. Rho, S. Kim, H. Suh, D. Kim, H. Kim, S. Lee, J. Park, H. Hwang, S. Hwang, J. Lee, Y. An, J. Yi, Y. Seo, D. Jung, M. Lee, S. Cho, Y. Kim, J. Rho, S. Park, S. Chung, J. Jeong, and S. Hong: Fully integrated 54nm STT-RAM with the smallest bit cell dimension for high density memory application. 304 (2010).
8. S. Ikeda, J. Hayakawa, Y.M. Lee, F. Matsukura, Y. Ohno, T. Hanyu, H. Ohno, Magnetic tunnel junctions for spintronic memories and beyond. IEEE Trans. Electron Devices **54**(5), 991 (2007)
9. S. Jung, H. Lee, S. Myung, H. Kim, S.K. Yoon, S.W. Kwon, Y. Ju, M. Kim, W. Yi, S. Han, B. Kwon, B. Seo, K. Lee, G.H. Koh, K. Lee, Y. Song, C. Choi, D. Ham, S.J. Kim, A crossbar array of magnetoresistive memory devices for in-memory computing. Nature **601**(7892), 211 (2022)
10. T. Leonard, S. Liu, M. Alamdar, H. Jin, C. Cui, O.G. Akinola, L. Xue, T.P. Xiao, J.S. Friedman, M.J. Marinella, C.H. Bennett, J.A.C. Incorvia, Shape-dependent multi-weight magnetic artificial synapses for neuromorphic computing. Adv. Electron. Mater. **8**(12), 1 (2022)
11. J. Grollier, D. Querlioz, K.Y. Camsari, K. Everschor-Sitte, S. Fukami, M.D. Stiles, Neuromorphic spintronics. Nat. Electron. **3**(7), 360 (2020)
12. K. Hayakawa, S. Kanai, T. Funatsu, J. Igarashi, B. Jinnai, W.A. Borders, H. Ohno, S. Fukami, Nanosecond random telegraph noise in in-plane magnetic tunnel junctions. Phys. Rev. Lett. **126**(11), 117202 (2021)
13. N.A. Aadit, A. Grimaldi, M. Carpentieri, L. Theogarajan, J.M. Martinis, G. Finocchio, K.Y. Camsari, Massively parallel probabilistic computing with sparse Ising machines. Nat. Electron. **5**(7), 460 (2022)
14. S. Yuasa, T. Nagahama, A. Fukushima, Y. Suzuki, K. Ando, Giant room-temperature magnetoresistance in single-crystal Fe/MgO/Fe magnetic tunnel junctions. Nat. Mater. **3**(12), 868 (2004)

15. S.S.P. Parkin, C. Kaiser, A. Panchula, P.M. Rice, B. Hughes, M. Samant, S.H. Yang, Giant tunnelling magnetoresistance at room temperature with MgO (100) tunnel barriers. Nat. Mater. **3**(12), 862 (2004)
16. S. Bhatti, R. Sbiaa, A. Hirohata, H. Ohno, S. Fukami, S.N. Piramanayagam, Spintronics based random access memory: a review. Mater. Today **20**(9), 530 (2017)
17. M. Barangi, P. Mazumder, Straintronics: a leap toward ultimate energy efficiency of magnetic random access memories. IEEE Nanotechnol. Mag. **9**(3), 15 (2015)
18. P. Li, A. Chen, D. Li, Y. Zhao, S. Zhang, L. Yang, Y. Liu, M. Zhu, H. Zhang, X. Han, Electric field manipulation of magnetization rotation and tunneling magnetoresistance of magnetic tunnel junctions at room temperature. Adv. Mater. **26**, 4320 (2014)
19. T. Jin, L. Hao, J. Cao, M. Liu, H. Dang, Y. Wang, D. Wu, J. Bai, F. Wei, Electric field control of anisotropy and magnetization switching in CoFe and CoNi thin films for magnetoelectric memory devices. Appl. Phys. Express **7**(4), 2–6 (2014). https://doi.org/10.7567/APEX.7.043002
20. E. Klokholm, J. Aboaf, The saturation magnetostriction of thin polycrystalline films of iron, cobalt, and nickel. J. Appl. Phys. **53**(3), 2661 (1982)
21. V. Sampath, N. D'Souza, G.M. Atkinson, S. Bandyopadhyay, J. Atulasimha, Experimental demonstration of acoustic wave induced magnetization switching in dipole coupled magnetostrictive nanomagnets for ultralow power computing. Appl. Phys. Lett. **109**(10), 102403 (2016)
22. M.S. Fashami, S. Bandyopadhyay, J. Atulasimha, Experimental clocking of nanomagnets with strain for ultralow power Boolean logic. Nano Lett. **16**(2), 1069–1075 (2016)
23. Z. Zhao, M. Jamali, N. D'Souza, D. Zhang, S. Bandyopadhyay, J. Atulasimha, J.-P. Wang, Giant voltage manipulation of MgO based magnetic tunnel junctions via localized anisotropic strain: a potential pathway to ultra-energy-efficient memory technology. Appl. Phys. Lett. **109**(9), 092403 (2016)
24. R. Wu, Origin of large magnetostriction in FeGa alloys. J. Appl. Phys. **91**(10), 7358 (2002)
25. K.P. Mohanchandra, S.V. Prikhodko, K.P. Wetzlar, W.Y. Sun, P. Nordeen, iG.P. Carman, Sputter deposited terfenol-D thin films for multiferroic applications. AIP Adv. (2015). https://doi.org/10.1063/1.4930602
26. J.L. Weston, A. Butera, T. Lograsso, M. Shamsuzzoha, I. Zana, G. Zangari, J. Barnard, Fabrication and characterization of Fe81Ga19 thin films. IEEE Trans. Magn. **38**(5), 2832 (2002)
27. D.B. Gopman, V. Sampath, H. Ahmad, S. Bandyopadhyay, J. Atulasimha, Static and dynamic magnetic properties of sputtered Fe – Ga thin films. IEEE Trans. Magn. **53**(11), 1 (2017)
28. Z. Zhang, Y. Wu, L. Sang, H. Wiu, J. Huang, Y. Takahashi, R. Li, S. Koizumi, M. Toda, I. Akita, Y. Koide, M. Liao, Coupling of magneto-strictive FeGa film with single crystal daimond MEMS resonator for high-reliability magnetic sensing at high temperature. Mater. Res. Lett. **8**, 180–186 (2020)
29. H.E. Sostman, Melting point of gallium as a temperature calibration standard. Rev. Sci. Instrum. **48**(2), 127 (2008)
30. J-P Wang and M. T Rahman: Magnetic Tunnel Junction Device. US Patent 8604572 (2013).
31. W.H. Butler, X.-G. Zhang, T.C. Schulthess, J.M. MacLaren, Spin-dependent tunneling conductance of Fe|MgO|Fe sandwiches. Phys. Rev. B **63**(5), 054416 (2001)
32. J. Hayakawa, S. Ikeda, F. Matsukura, H. Takahashi, H. Ohno, Dependence of giant tunnel magnetoresistance of sputtered CoFeB/MgO/CoFeB magnetic tunnel junctions on MgO barrier thickness and annealing temperature. Jpn. J. Appl. Phys. (2005). https://doi.org/10.1143/JJAP.44.L587
33. D.D. Djayaprawira, K. Tsunekawa, M. Nagai, H. Maehera, S. Yamagata, N. Watanbe, S. Yuasa, Y. Suzuki, K. Ando, 230% room-temperature magnetoresistance in CoFeB/MgO/CoFeB magnetic tunnel junctions. Appl. Phys. Lett. **86**, 092502 (2005)
34. D.C. Worledge, P.L. Trouilloud, Magnetoresistance measurement of unpatterned magnetic tunnel junction wafers by current-in-plane tunneling. Appl. Phys. Lett. **83**(1), 84 (2003)
35. K. Yakushiji, A. Fukushima, H. Kubota, M. Konoto, S. Yuasa, Ultralow-voltage spin-transfer switching in perpendicularly magnetized magnetic tunnel junctions with synthetic antiferromagnetic reference layer. Appl. Phys. Exp. (2013). https://doi.org/10.7567/APEX.6.113006
36. S. Tegen, I. Mönch, J. Schumann, H. Vinzelberg, C.M. Schneider, Effect of Néel coupling on magnetic tunnel junctions. J. Appl. Phys. **89**(12), 8169–8174 (2001)